ENVIRONMENTAL ENGINEERING SCIENCE
Volume 19, Number 6, 2002

Influence of Crossflow Membrane Filter Geometry and Shear Rate on Colloidal Fouling in Reverse Osmosis and Nanofiltration Separations

Eric M.V. Hoek,[1]* Albert S. Kim,[2] and Menachem Elimelech[3]

[1]Department of Chemical and Environmental Engineering
University of California
Riverside, CA 92521
[2]Department of Civil and Environmental Engineering
University of Hawaii at Manoa
Honolulu, HI 96822
[3]Department of Chemical Engineering, Environmental Engineering Program
Yale University
New Haven, CT 06520

ABSTRACT

A laboratory-scale crossflow membrane filtration apparatus was designed to investigate the relative influence of filter geometry and shear rate on colloidal fouling of reverse osmosis (RO) and nanofiltration (NF) membranes. An expression that allows clarification of the mechanisms of flux decline due to colloidal fouling in RO and NF separations was derived by combining the solution-diffusion model, film-theory, and a modified cake filtration model. With this new fouling model, the interplay between the salt concentration polarization layer and a growing colloid deposit layer may be quantified. The hydraulic pressure drop across a colloid deposit layer was shown to be negligible compared to cake-enhanced osmotic pressure. The difference in flux decline observed in filters with different channel heights resulted from different cake layer thickness, and thus, different cake-enhanced osmotic pressure. A moderate reduction in the initial concentration polarization and cake-enhanced osmotic pressure was obtained by operating at a higher shear rate within a given filter. However, thicker cakes were produced in the filter with greater channel height regardless of crossflow hydrodynamics, which resulted in greater loss of flux. In all modes of operation for either channel height, salt rejection decreased in proportion to the extent of flux decline. By decreasing channel height, both flux and salt rejection were enhanced by reducing all fouling mechanisms—salt concentration polarization, cake layer resistance, and the cake-enhanced osmotic pressure.

Key words: reverse osmosis; nanofiltration; film-theory; mass transfer; membrane fouling; colloidal fouling; osmotic pressure; concentration polarization; cake resistance

*Corresponding author: University of California, Department of Chemical and Environmental Engineering, Riverside, CA 92521. *Phone*: 909-787-7345; *Fax*: 909-787-5696; *E-mail*: hoek@engr.ucr.edu

INTRODUCTION

THE PERFORMANCE OF REVERSE OSMOSIS (RO) and nanofiltration (NF) membranes has been studied extensively in terms of operating conditions, module geometry, and treatment train configuration (Sirkar and Rao, 1981; Sirkar *et al.*, 1982; Evangelista, 1985; Wiley *et al.*, 1985; Kataoka *et al.*, 1991; Van Der Meer and Van Dijk, 1997; Voros *et al.*, 1997; Zhu *et al.*, 1997; Maskan *et al.*, 2000). Of considerable importance to all of these studies is the influence of mass transfer on the buildup of rejected ionic species at the membrane surface, or concentration polarization (CP). High-concentration polarization increases the salt concentration at the membrane surface, which results in lower salt rejection and higher *trans*-membrane osmotic pressure, and thus, a reduction in performance. Many past performance studies specifically focused on optimizing crossflow hydrodynamics and/or membrane filter geometry to limit salt CP and the associated loss of performance due to osmotic pressure buildup (Sirkar and Rao, 1981; Sirkar *et al.*, 1982; Evangelista, 1985; Wiley *et al.*, 1985; Van Der Meer and Van Dijk, 1997; Voros *et al.*, 1997; Zhu *et al.*, 1997; Maskan *et al.*, 2000). However, the use of RO/NF membranes in water treatment processes is further hindered because even pretreated feed waters may contain dissolved natural organic matter and small colloids composed of natural silica, clays, aggregated organics, or biologic matter, in addition to ionic constituents (Mallevialle *et al.*, 1996; Hong and Elimelech, 1997; Zhu and Elimelech, 1997; Braghetta *et al.*, 1998; Chellam and Taylor, 2001). Therefore, the additional pressure drop due to biologic, colloidal, or organic matter fouling must be rigorously incorporated into RO/NF performance models to accurately predict the transient loss of flux and associated decline in salt rejection.

Incorporation of colloidal fouling into RO/NF performance models is not trivial because the fundamental mechanisms are not well-understood. What is known comes predominantly from research on colloidal fouling of microfiltration and ultrafiltration membranes. Salt concentration has been shown to exacerbate colloidal fouling for RO and NF membranes (Zhu and Elimelech, 1997; Braghetta *et al.*, 1998; Yiantsios and Karabelas, 1998), but little is known about the nature of colloid–solute interactions within the salt CP layer. It was recently demonstrated that a growing colloid deposit layer may exacerbate concentration polarization for salt rejecting membranes, and cause far more flux decline than could be explained by the hydraulic resistance of the colloid deposit layer alone (Hoek, 2002; Hoek and Elimelech, 2002). The experimental data suggested that the primary mechanism of fouling was hindered back-diffusion of salt ions within the colloid deposit layers leading to a "cake-enhanced osmotic pressure." Therefore, it is hypothesized that the decline in performance associated with colloidal fouling may be controlled by optimizing mass transfer, and this is tested by investigating the relative influence of crossflow membrane filter geometry and hydrodynamics.

In this investigation, the combined "solution diffusion–film-theory" model is used to describe the influence of crossflow membrane filter geometry and crossflow hydrodynamics on initial salt concentration polarization. This solute transport-CP model is further combined with a modified cake filtration model to provide a simple analytical expression that allows simultaneous estimation of cake layer porosity and the cake-enhanced osmotic pressure from experimental fouling data. A laboratory-scale crossflow membrane filtration apparatus was designed specifically to investigate the relative influence of filter geometry and crossflow hydrodynamics on colloidal fouling of salt rejecting membranes. Measurement of colloid deposit layer mass during several filtration experiments verified the relative insignificance of cake layer hydraulic resistance, and revealed valuable insight into the role of channel height and shear rate in colloidal fouling of membranes.

THEORETICAL

Solute transport and concentration polarization

The starting point for our mathematical description of RO/NF separations is the solution–diffusion model. The model assumes that the permeation driving force is the gradient in chemical potential of the solute (Wijmans and Baker, 1995). When the transport equation is expressed in terms of solvent flux (J), it is given as

$$J = A(\Delta P - \sigma\Delta\Pi), \tag{1}$$

where A is the solvent permeability through the membrane, ΔP is the applied pressure, $\Delta\Pi$ is the osmotic pressure difference between the membrane surface and the permeate, and σ is the reflection coefficient. The reflection coefficient represents the intrinsic salt rejection by the membrane, but when intrinsic salt rejection is over ca. 0.98, which is typical for reverse osmosis separations, σ may be assumed equal to unity (Bhattacharjee *et al.*, 2001). When intrinsic salt rejection is significantly less than 0.98 (i.e., nanofiltration), the reflection coefficient should be used to more accurately predict the resultant *trans*-membrane osmotic pressure (Murthy and Gupta, 1997). The combined product of $\sigma\Delta\Pi$ may be thought of as the "effective *trans*-membrane" osmotic pressure drop, which will be denoted as $\Delta\pi_m$ in this study. Equation (1)

serves as the starting point for the design of most modern RO/NF separations.

The rejection of ionic species results in an elevated salt concentration near the membrane surface. The high solute concentration at the membrane surface decays back to the bulk ionic concentration over some distance, defined as the concentration polarization (CP) layer "thickness." In crossflow membrane filtration, the CP layer quickly reaches a steady state, and the transverse solute flux through the CP layer is constant. The solvent flux (J) may then be determined by the following one-dimensional, steady-state mass balance across the CP layer:

$$JC - D\frac{dC}{dy} = JC_p, \tag{2}$$

where C is the solute concentration, D is the solute diffusivity, C_p is the solute permeate concentration, and y is the distance measured normal to and away from the membrane surface (Zydney, 1997).

Integrating Equation (2) over the salt concentration polarization layer thickness (δ) with the appropriate boundary conditions ($y = 0$, $C = C_m$; $y = \delta$, $C = C_b$) results in

$$J = \frac{D}{\delta}\ln\left(\frac{C_m - C_p}{C_b - C_p}\right), \tag{3}$$

where C_m is the membrane surface salt concentration and C_b is the bulk salt concentration. This expression can be rearranged to provide a direct estimation of the concentration polarization modulus (C_m/C_b) from

$$\frac{C_m}{C_b} = (1 - R_o) + R_o \exp\left(\frac{J}{k}\right). \tag{4}$$

Here, R_o is the observed rejection ($=1 - C_p/C_b$) and $k(=D/\delta)$ is the mass transfer coefficient. Alternate rearrangement of Equation (3) allows estimation of the effective *trans*-membrane osmotic pressure from

$$\Delta\pi_m = 2C_bRTR_o \exp\left(\frac{J}{k}\right), \tag{5}$$

where T is absolute temperature and R is the universal gas constant. The constant, 2, accounts for a 1:1 electrolyte solution at concentrations where van't Hoff's law is valid, which is the case for the experiments performed in this investigation. It is clear from Equation (5) that $\Delta\pi_m$ increases when bulk salt concentration, rejection, and flux increase. Further, maintaining high mass transfer coefficient is critical for optimal operation of RO/NF processes.

"Film-theory" model

Attempts to predict either the concentration polarization modulus (C_m/C_b) or the *trans*-membrane osmotic pressure ($\Delta\pi_m$) have traditionally been limited to mass transfer analogies of the heat transfer correlations for development of a stagnant film layer—sometimes referred to as "film-theory" models (Blatt *et al*., 1970). More fundamental models of concentration polarization exist (Song and Elimelech, 1995; Elimelech and Bhattacharjee, 1998; Bhattacharjee *et al*., 1999, 2001), but film theory provides a simple analytical approach that works well for most RO/NF separations. Therefore, film theory serves as the design basis for most modern reverse osmosis processes.

For laminar flow in a thin rectangular channel, the "film-theory" mass transfer coefficient (k_f) may be related to the Sherwood number (Sh) through the following equation:

$$\mathrm{Sh} = k_f\frac{d_h}{D} = 1.62\left(\mathrm{Re\ Sc}\ \frac{d_b}{L_c}\right)^{1/3}, \tag{6}$$

where Re is the Reynolds number ($=ud_h/\nu$, with u being the bulk crossflow velocity and ν the solution kinematic viscosity), d_h is the channel hydrodynamic diameter ($\approx 2H_c$, with H_c being the channel height), Sc is the Schmidt number (ν/D), and L_c is the channel length (Porter, 1972).

By expanding the individual components and rearranging, the mass transfer coefficient is shown to depend on flow rate, channel geometry, and solute type via

$$k_f = 1.62\left(\frac{QD^2}{2W_cH_c^2L_c}\right)^{1/3} = 1.62\left(\frac{uD^2}{2H_cL_c}\right)^{1/3} = 1.62\left(\frac{\gamma_0D^2}{12L_c}\right)^{1/3}. \tag{7}$$

Here, Q is the feed flow rate, W_c is the channel width, and γ_0 is the wall shear rate. The shear rate represents the velocity gradient (du/dy) through a laminar hydrodynamic boundary layer and can be estimated directly from $6Q/W_cH_c^2$ in a thin rectangular channel (Davis, 1992).

From Equation (7) it is clear that for a given solute, mass transfer is most significantly enhanced by reducing channel height (H_c), and to a lesser extent by increasing crossflow. It is this relationship that provides the logical basis for testing the relative influence of crossflow rate and channel height on colloidal fouling. For this study, the preferred form of Equation (7) contains the shear rate (γ_0) because it captures the influences of both crossflow rate and channel height in a single term.

Cake filtration model

The mechanism of flux decline associated with colloid deposition on a membrane surface is typically modeled through the phenomenologic "cake filtration" model, which was originally developed for microfil-

tration separations (Davis, 1992). The transient flux is described by

$$J(t) = \frac{\Delta p}{R_m + R_c(t)} \tag{8a}$$

where the solvent flux, J, is a function of the net (or effective) applied pressure, $\Delta p(=\Delta P - \Delta\pi_m)$, the membrane hydraulic resistance, R_m, $(=1/A)$, and the cake layer resistance, R_c (Faibish *et al.*, 1998). Flux at constant pressure is solely governed by the product of a constant specific cake resistance (α) and transient deposit layer mass per unit membrane area (M_d) as

$$R_c(t) = \alpha M_d(t) = \left[\frac{45\ \mu_0(1-\varepsilon)}{\rho_p a_p^2 \varepsilon^3} \right] M_d(t), \tag{8b}$$

where μ_0 is the solvent viscosity, ε is the cake layer porosity, a_p is the particle radius, and ρ_p is the particle density. The specific cake resistance (the term in brackets) cannot be determined *a priori* without knowing the cake layer porosity. However, the following discussion leads to an analytical expression for directly estimating cake layer porosity and cake-enhanced osmotic pressure from known constants and experimentally measurable parameters.

Cake-enhanced osmotic pressure model

In the standard cake filtration model, the transient flux decline (or decline in *trans*-membrane pressure) is assumed to arise solely from the added hydraulic resistance of the cake layer. However, it was previously demonstrated that this is an unreasonable assumption for salt rejecting membranes because the primary mechanism of the flux decline is a transient, cake-enhanced osmotic pressure (Hoek, 2002). The cake-enhanced osmotic pressure model begins by rearranging the cake filtration equation into a series of pressure drops

$$\Delta p_m(t) = \Delta P - \Delta\pi_m{}^*(t) - \Delta p_c(t) \tag{9a}$$

where the cake-enhanced osmotic pressure is described by,

$$\Delta\pi_m{}^*(t) = \Delta P - J(t)R_m - J(t)\left[\frac{45\mu(1-\varepsilon)}{\rho_p a_p^2 \varepsilon^3} \right] M_d(t). \tag{9b}$$

The transient driving force for permeation, the *trans*-membrane pressure (Δp_m) is a function of the constant applied pressure (ΔP), the transient cake-enhanced osmotic pressure ($\Delta\pi_m{}^*$), and the transient *trans*-cake hydraulic pressure (Δp_c).

It is hypothesized that for thin cake layers (compared to the film layer thickness), the cake-enhanced osmotic pressure results solely from the hindered back-diffusion of salt ions trapped within the colloid-cake layer (Hoek, 2002). Figure 1 illustrates this effect. With no particles deposited (top), the solute concentration polarization layer quickly reaches steady state, whereby solute transport by convection towards the membrane (minus that which permeates) is balanced by solute back-transport by diffusion. As particles accumulate and form a thin cake layer over the surface of the membrane (bottom), the diffusion of salt ions back into the bulk is hindered because of the tortuous path the ions must follow to circumnavigate the deposited colloids. Hindered back-diffusion of salt ions trapped in the cake layer leads to an enhanced membrane surface salt concentration ($C_m{}^*$) and, thus, enhanced osmotic pressure drop across the membrane ($\Delta\pi_m{}^*$).

The mathematical model that follows is based on three important assumptions. First, the cake layer is thin compared to the salt film-layer thickness. Past investigations have shown that the tangential flow field is relatively unaffected when the cake layer is thin with respect to the channel height (Faibish *et al.*, 1998) because the cake layer does not occupy a significant fraction of the chan-

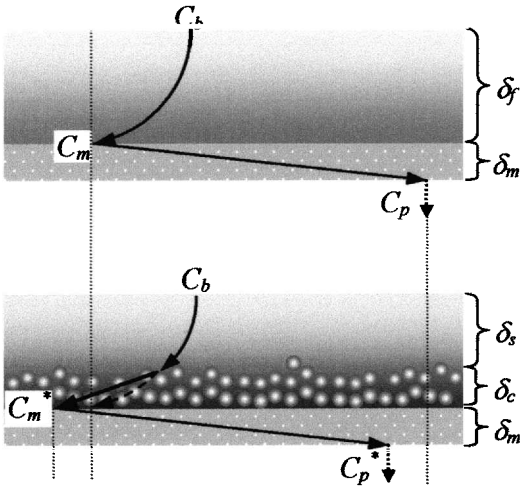

Figure 1. Conceptual illustration of "cake-enhanced osmotic pressure" effect. In the absence of a colloid deposit layer (top figure), the elevated concentration at the membrane surface (C_m) decays to the bulk concentration (C_b) over the salt concentration polarization (film) layer thickness (δ_f). The salt concentration drops across the membrane thickness (δ_m) due to salt rejection. For a thin deposit layer (bottom figure), the film layer thickness remains constant and the difference between δ_f and cake thickness (δ_c) is δ_s. In the presence of a colloid deposit layer the membrane surface salt concentration is enhanced ($C_m{}^*$) due to hindered back-diffusion of salt ions and a decrease in salt rejection results. The elevated $C_m{}^*$ will also result in elevated permeate salt concentration, $C_p{}^*$.

nel cross section (Davis, 1992). Crossflow shear rate is relatively unaffected by the presence of the cake layer, and thus the CP layer thickness remains at the film thickness determined prior to particle deposition. Second, the colloid deposit layer does not reject salt ions, so the profile of salt concentration above the colloid deposit layer is unchanged from that prior to cake formation. Third, the effective diffusion coefficient for salt ions trapped within the colloid deposit layer can be estimated with knowledge of the cake layer porosity.

A simple analytical expression for estimating the dependence of the hindered diffusion coefficient (D^*) on porosity is given by

$$D^* = (\varepsilon/\tau)\, D, \tag{10}$$

where D is the solute diffusivity in the bulk, ε is the porosity, and $\tau(\approx 1 - \ln\varepsilon^2)$ is the diffusive tortuosity (Boudreau, 1996). Recent investigations have shown that cake layer porosities for silica colloids filtered under similar physical and chemical conditions were typically in the range of 0.3 to 0.7 (Faibish *et al.*, 1998; Yiantsios and Karabelas, 1998; Endo and Alonso, 2001). The ratio of the effective diffusion coefficient to the bulk diffusion coefficient is plotted against cake layer porosity in Fig. 2. Over the range of typical porosity values the effective diffusion coefficient may be reduced to between 10 and 40% of the bulk diffusion coefficient, which results in significantly enhanced salt concentration at the membrane surface.

Next, the effective mass transfer coefficient is broken down into two parts—one describing mass transfer through the colloid deposit layer and one describing mass transfer from the interface of the colloid layer back into the bulk. The resulting "hindered" mass transfer coefficient (k^*) is estimated from

$$\frac{1}{k^*} = \frac{\delta_c}{D^*} + \frac{\delta_s}{D}, \tag{11}$$

where δ_c is the colloid deposit layer thickness and δ_s is the difference between the film (δ_f) and cake layer thicknesses. Equation (11) comes directly from integrating Equation (2) separately across the cake and CP layers. Even if the cake layer is very thin ($\delta_c << \delta_s$) the cake-enhanced osmotic pressure may be significant because the hindered diffusion coefficient can be an order of magnitude smaller than the bulk diffusion coefficient.

Because the film layer thickness was assumed constant, the salt layer thickness over the cake is the difference between the original film thickness and the cake thickness (i.e., $\delta_s = \delta_f - \delta_c$). Note that the cake layer thickness can be written in terms of cake mass per unit membrane area as $\delta_c = M_d/\rho_p(1 - \varepsilon)$ (Faibish *et al.*, 1998). Rewriting Equation (11), the hindered mass transfer coefficient expression, in terms of δ_f and δ_c and substituting into Equation (5), results in the following expression for the cake-enhanced osmotic pressure:

$$\Delta\pi_m^* = 2C_bRTR_o \exp\left[\frac{J}{k_f} + \frac{JM_d}{\rho_p(1-\varepsilon)}\left(\frac{1 - \ln(\varepsilon^2)}{D_\infty\varepsilon} - \frac{1}{D_\infty}\right)\right]. \tag{12}$$

All parameters in this equation are constant or experimentally measurable, except cake porosity (ε) and cake-enhanced osmotic pressure ($\Delta\pi_m^*$). Setting Equation (12) equal to Equation (9b) allows direct calculation of the cake layer porosity, and thus, cake-enhanced osmotic pressure.

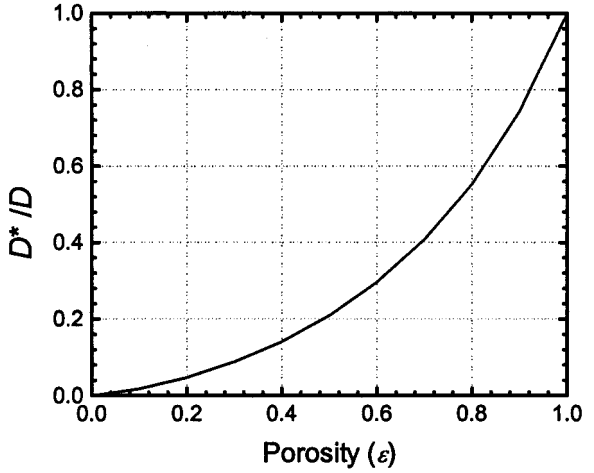

Figure 2. Ratio of the cake-hindered salt diffusion coefficient to the bulk diffusion coefficient predicted by Equation (10) for a range of cake layer porosities.

MATERIALS AND METHODS

Membranes

Four commercial RO/NF polyamide thin-film composite membranes were used in this study. The RO membranes were Hydranautics LFC1 (Oceanside, CA) and Trisep X20 (Goleta, CA). The NF membranes were Dow-FilmTec NF70 (Minneapolis, MN) and Osmonics HL (Minnetonka, MN). All membranes were stored in deionized water at 5°C with water replaced regularly. The membranes were characterized for relevant performance properties such as pure water permeability (A) and observed salt rejection (R_o). Salt rejection experiments were conducted at 0.01 M NaCl and unadjusted pH of 6.8 ± 0.2, which are the same feed conditions used in all fouling experiments. All four membranes are thought to be

moderately negatively charged (−15 to −25 mV) at typical solution chemistries based on streaming potential analyses reported elsewhere (Vrijenhoek *et al.*, 2001).

Reagents and model colloids

Salt stock solutions were prepared using ACS grade NaCl (Fisher Scientific, Pittsburgh, PA) dissolved in deionized water (Nanopure Infinity Ultrapure, Barnstead, Dubuque, IA). Nissan Chemical America Corporation (Houston, TX) provided the colloidal particles used in the fouling experiments. The particles were certified as 0.10 μm ($\pm$0.03 μm) silica particles in an aqueous suspension. Chemical analysis by the manufacturer indicates the suspension to be 40.7% (w/w) amorphous silica with a specific gravity of 1.3. Based on the specific gravity and weight percent of the suspension the particle density was calculated to be 2.36 g/cm^3. Gravimetric analysis of the particle suspension revealed the particle density to be 2.11 g/cm^3, which compares well with the above calculation and other reported values (Faibish *et al.*, 1998). Particles were negatively charged (−25 mV) at pH 6.8 $\pm$ 0.2 and 0.01 M NaCl as determined from electrophoretic mobility measurements reported elsewhere (Vrijenhoek *et al.*, 2001).

Laboratory-scale crossflow membrane filters

The test apparatus was a modified version of two commercially available stainless steel crossflow membrane filtration (CMF) units (Sepa CF, Osmonics, Inc.; Minnetonka, MN). The crossflow membrane filtration units are rated for operating pressures up to 6895 kPa (1000 psi). Both crossflow units have dimensions of 14.6 and 9.5 cm for channel length (L_c) and width (W_c), respectively, while the channel heights (H_c) are 34 mil (0.86 mm) and 68 mil (1.73 mm), respectively. The two crossflow membrane filtration units will hereafter be described simply as the "34" and "68" units, thus indicating their respective channel heights. These channel dimensions provide an effective membrane area (A_m) of 1.39×10^{-2} m^2 per unit and cross-sectional flow areas (A_x) of 0.82×10^{-4} m^2 for the 34 unit and 1.64×10^{-4} m^2 for the 68 unit. The applied pressure (ΔP) was constant and monitored by a pressure gage (Cole-Parmer, Chicago, IL) and flux was monitored in real time by a digital flow meter (Optiflow 1000, Humonics; Rancho Cordova, CA). Specific modifications to the manufacturer's setup were reported elsewhere (Vrijenhoek *et al.*, 2001); a schematic diagram of the experimental system is presented in Fig. 3.

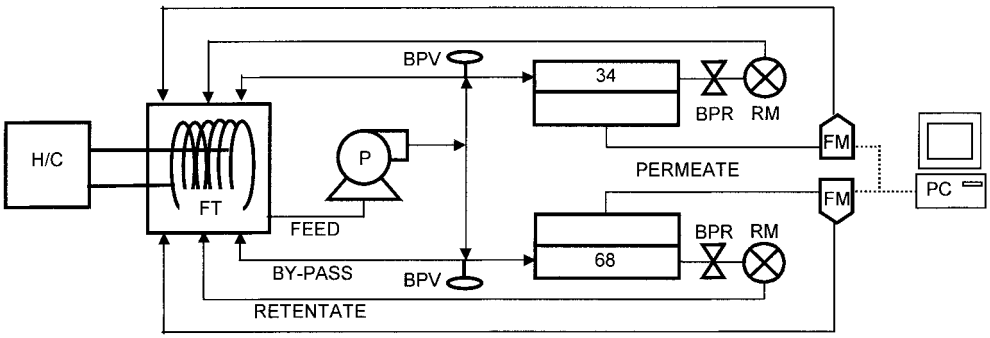

KEY

Symbol	Description
H/C	recirculating heater/chiller
FT	feed tank
P	feed pump
BPV	by-pass valve
34	CMF test cell with 34 mil (0.864 mm) channel height
68	CMF test cell with 68 mil (1.727 mm) channel height
BPR	back-pressure regulator
RM	floating disk rotameter (crossflow rate)
FM	digital flow meter (permeate flow rate)
PC	laboratory computer

Figure 3. Crossflow membrane filtration (CMF) apparatus used in experiments designed to simultaneously test the influence of crossflow hydrodynamics and membrane filter geometry on colloidal fouling. The two crossflow membrane filters may be fed in parallel from a common feed tank, or individually.

Measuring membrane hydraulic resistance

Different membrane coupons were used for each filtration experiment, so the membrane hydraulic resistance was determined prior to each fouling experiment. First, deionized (DI) water was circulated at 250 psi (1724 kPa) for up to 24 h to dissociate flux decline due to membrane compaction (and other unknown causes inherent of lab-scale recirculation systems). Flux was monitored continuously for the duration of the experiment and recorded in real time on a laboratory computer. After DI equilibration, the pressure was changed in increments of 50 psi (345 kPa), from a high of 250 psi to a low of 50 psi and flux recorded at a feed flow rate of 0.95 liters per minute (Lpm). At each pressure, flux was monitored for at least 30 min to ensure stable performance. The crossflow was then increased to 1.90 Lpm and flux was recorded at 50 psi increments from 50 to 250 psi. Finally, feed flow rate was set at 3.79 Lpm and the flux was recorded at 50 psi increments from 250 psi down to 50 psi. At each crossflow and pressure the average of all of the stable flux measurements was plotted against applied pressure. The slope of a line fitted to pure water flux vs. pressure data by a least-squares linear regression provided the membrane hydraulic resistance. As expected, there was no measured influence of feed flow rate on pure water flux for any experiments, but the procedure provided extra data points for the regression analysis. The pH of feed was monitored throughout the pure water flux experiments to ensure constant feed solution chemistry.

Measuring CP modulus and initial osmotic pressure drop

After the membrane pure water hydraulic resistance (R_m) was determined, concentration polarization effects could be quantified using film-theory and the velocity variation technique described herein. An appropriate volume of 1 M stock NaCl solution was added to the feed tank to provide the desired experimental ionic strength. The same feed solution ionic strength (0.01 M) was used for all filtration experiments in this study. The sequence of varying applied pressure and feed flow rate was repeated. The effective osmotic pressure drop across the membrane ($\Delta\pi_m$) for each velocity variation was determined from Equation (1) with $A = 1/R_m$. Each combination of pressure and flow yielded different permeate and crossflow velocities, respectively, and hence the description as the "velocity variation" technique. The experimental film-theory mass transfer coefficient was calculated from the measured $\Delta\pi_m$ and Equation (5), and then the experimental CP modulus was calculated from Equation (4) for each velocity variation. The feed solution pH was monitored throughout the salt water experiments to ensure stable feed conditions. Observed salt rejection (R_o) was determined by measuring feed and permeate conductivity. Conductivity was determined to be linearly proportional to NaCl concentration by performing a least-squares linear regression of conductivity measurements for solutions with known NaCl concentrations.

Measuring decline in flux and salt rejection due to colloidal fouling

After the salt water experiments were finished, pressure and crossflow were adjusted to produce the desired initial flux and wall shear for the fouling experiment. After stable performance (flux and salt rejection) was achieved for a minimum of 60 min, a dose of silica particles was added to the feed tank to provide the appropriate particle feed concentration. The concentration of 100 nm silica particles was 0.008% (v/v), which yielded an average turbidity of 53.2 NTU. The same concentration of particles was used in all colloidal fouling experiments performed for this study. Conductivity, pH, and turbidity measurements were made at the start, end, and at several points during the fouling experiment to determine salt rejection, to ensure complete rejection of particles, and to ensure feed conditions were constant throughout the test. The transient flux at constant pressure was downloaded in real time from the digital permeate flow meter to a laboratory computer.

Measuring colloid deposit layer mass

In some experiments, the mass of colloid deposit layers was measured using a previously published technique (Faibish *et al*., 1998). The feed tank volume was reduced such that the mass of particles dosed into the feed tank would be measurably reduced by the mass of particles accumulated in the cake layer over the membrane. A smaller feed volume was used for these experiments such that a small, but measurable decrease in feed turbidity occurred within in the time scale of the experiment. In these experiments only one crossflow filter was used so that the decline in feed suspension turbidity was related to a single crossflow membrane filter. No significant difference in mass transfer parameters, flux decline data, or salt rejection data was found when compared to data from experiments using constant feed particle concentration fed in parallel to both crossflow membrane filters. The measured colloid deposit layer mass was then combined with other relevant measured and constant parameters into Equations (9) and (12) to determine the cake porosity and cake-enhanced osmotic pressure.

RESULTS AND DISCUSSION

Predicted and measured concentration polarization effects

The film-theory predicted mass transfer parameters for the lab-scale CMF units are provided in Table 1. The listed volumetric feed flow rates (Q) are those used in fouling experiments and the data are arranged in order of decreasing CP modulus. Velocity, shear rate, and Reynolds number all increase with increasing feed flow. However, at a given volumetric flow rate, velocity is doubled as d_h is halved, so the Reynolds number is the same in either channel. The wall shear rate captures both the difference in channel geometry and crossflow, and so it can be made identical in the two units at certain crossflow rates. The mass transfer coefficients, CP moduli, and osmotic pressure drops predicted from the film-theory equations all increase in proportion to the change in shear rate, again highlighting the usefulness of this parameter. The theoretical film layer thickness was calculated from $k_f = D/\delta_f$ using 1.611×10^{-9} $m^{2/s}$ as the diffusion coefficient for NaCl, and ranged from about 50 to 125 μm. The most important data from Table 1 are items 3 and 4. The shear rate is identical, so the film-theory predicted mass transfer parameters (k_f, δ_f, C_m/C_b, and $\Delta\pi_m$) are identical.

The theoretical and experimental concentration polarization moduli for the crossflow membrane filters are plotted against crossflow Reynolds number in Fig. 4. Experimentally determined salt rejection is labeled next to each experimental data point. The labels 1 to 6 correspond to the same item numbers in Table 1. The experimental osmotic pressure drop was determined at a stable flux of 1.42×10^{-5} m/s (30 gfd) and combined with observed salt rejection data in Equation (5) to calculate the experimental mass transfer coefficient. The experimental CP modulus was then calculated from Equation (4). The theoretical concentration polarization modulus data plotted in Fig. 4 was calculated from Equation (4) using the experimental salt rejection values at the corresponding Reynolds flows and linearly interpolating (or extrapolating) salt rejection values for flow rates in between (or beyond). The theoretical CP modulus was relatively insensitive to R_o over the range of experimentally observed rejection values in Fig. 4, so this simple linear interpolation should not introduce significant error.

Both the predicted and experimental concentration polarization effects are shown to be more severe in the 68 unit than in the 34 unit over the entire range of flow rates. The experimental data are in fairly good agreement with predicted CP modulus data, although the experimental data appear relatively flat over the range of Reynolds numbers. This may be due in part to the fact that wall-suction (permeation) is ignored in the film-theory predicted mass transfer coefficient. In items 3 and 4 of Table 1, the hydrodynamic conditions are predicted to yield the same CP modulus in the two filters, but experimental CP moduli differed by about 17%. This film-theory "error" may be due to entrance and side-wall effects not accounted for in film theory predictions, as well as other potential, unknown experimental errors.

Figure 5 presents the predicted *trans*-cake hydraulic pressures, cake-enhanced osmotic pressures, and permeate fluxes in the 34 and 68 units for varied cake layer thickness and porosity. Hydrodynamic conditions were those described in items 1 and 4 of Table 1. However, because the mass transfer parameters are identical in items 3 and 4, the 34 unit curves displayed in Fig. 5 theoretically represent the cake-enhanced osmotic pressures for the 68 unit under the conditions of item 3 in Table 1.

At a feed flow rate of 0.95 Lpm the initial *trans*-membrane osmotic pressures were about 14 and 21 psi in the

Table 1. Film-theory predicted mass transfer parameters for experimental CMF units.

Item no.	*CMF*[a] *unit*	Q[b] *[Lpm]*	u[c] *[cm/s]*	γ_0[d] *[s^{-1}]*	Re[e] *[−]*	k_f *[μm/s]*	δ_f *[μm]*	C_m/C_b[f] *[−]*	$\Delta\pi_m$[g] *[psi]*
1	68	0.95	9.6	334	372	13	126	3.0	21
2	68	1.89	19.2	668	745	16	100	2.4	17
3	68	3.79	38.4	1,336	1,489	20	79	2.0	14
4	34	0.95	19.2	1,336	372	20	79	2.0	14
5	34	1.89	38.4	2,671	745	26	63	1.7	12
6	34	3.79	76.9	5,342	1,489	32	50	1.5	11

Operation conditions used in the calculations are $J_0 = 1.42 \times 10^{-5}$ m/s (30 gfd), $C_b = 0.01$ M NaCl, and $R_o = 98\%$; [a]Channel height (H_c) = 0.864 mm (34) and 1.73 mm (68); channel length (L_c) = 146 mm; channel width (W_c) = 95 mm; [b]Q = volumetric feed flow rate in liters per minute (Lpm); [c]$u = Q/A_x$, A_x = channel cross-sectional area; [d]$\gamma_0 = 6u/H_c$ and is the channel wall shear rate; [e]$Re = ud_h/\nu$ and is the channel crossflow Reynolds number, $d_h = 2H_c$, ν = kinematic viscosity; [f]concentration polarization (CP) modulus calculated from Equation (4); [g]effective *trans*-membrane osmotic pressure calculated from Equation 5.

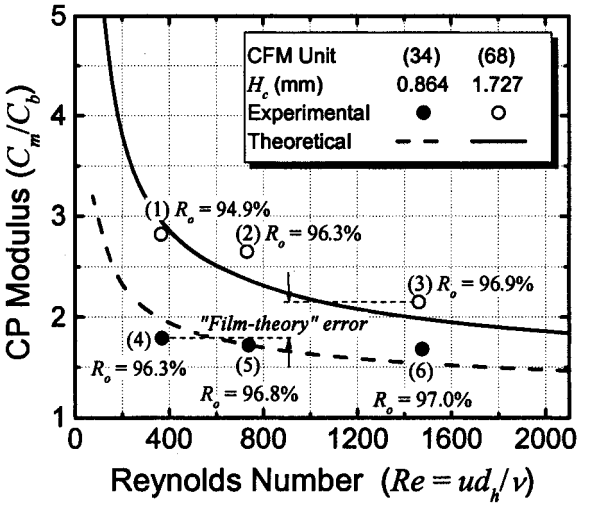

Figure 4. Comparison of theoretical and experimental concentration polarization (CP) modulus (C_m/C_b) vs. Reynolds number for the lab-scale CMF units. The numbers in parentheses correspond to the item numbers in Table 1. According to the "film-theory" predictions, the CP modulus should be the same for experiments 3 and 4. Both predicted and experimental CP modulus values were determined at $J_0 = 1.42 \times 10^{-5}$ m/s (30 gfd), $C_b = 0.01$ M NaCl, pH = 6.8 ± 0.2, and 25°C.

34 and 68 CMF units, respectively. *Trans*-cake hydraulic pressure (Δp_c) was determined from JR_c, where the cake resistance was obtained from the cake thickness, instead of cake mass [recall Equation (8b)], by the relation $\delta_c = M_d/\rho_p(1 - \varepsilon)$ (Faibish *et al.*, 1998). Note that there was a very subtle difference in *trans*-cake hydraulic pressure between the 34 and 68 units because the flux was different, but difference was negligible with respect to all other pressures. Cake-enhanced osmotic pressure ($\Delta\pi_m$*) was calculated from Equation (12). The salt rejection was linearly varied from 97 to 96% and 96 to 95% as cake layer increased from 0 to 25 μm in the 34 and 68 units, respectively.

Flux was determined iteratively to account for the interrelated effects of cake layer hydraulic pressure drop, osmotic pressure drop, and salt rejection at each theoretical cake thickness. At the initial flux of 1.42×10^{-5} m/s (30 gfd), Δp_c and $\Delta\pi_m$* were predicted from Equations (9) and (12), and a new flux was determined by solving Equation (9a) using the predicted Δp_c and $\Delta\pi_m$*. This flux was then used to recalculate the predicted Δp_c and $\Delta\pi_m$*. The calculations were performed iteratively until the flux value used in Equations (9) and (12) was returned equally by Equation (9a) to six significant figures. This allowed for accurate prediction of pressure drops and flux by accounting for the declining flux at each cake thickness.

In Fig. 5, the hydraulic pressure drop across the cake layer increased approximately linearly with cake layer thickness, such that a cake thickness of 25 μm accounted for a pressure drop between 1 and 5 psi. The cake-enhanced osmotic pressure increased from the initial osmotic pressure drop by as much as 40 psi in the 68 unit at the lowest porosity. The cake-enhanced osmotic pressure in the 68 unit is 1.5 times greater than that in the 34 unit across the entire range of cake thicknesses and for all three porosity values. However, this proportional difference yields flux decline that is always more severe in the 68 unit because the actual cake-enhanced osmotic

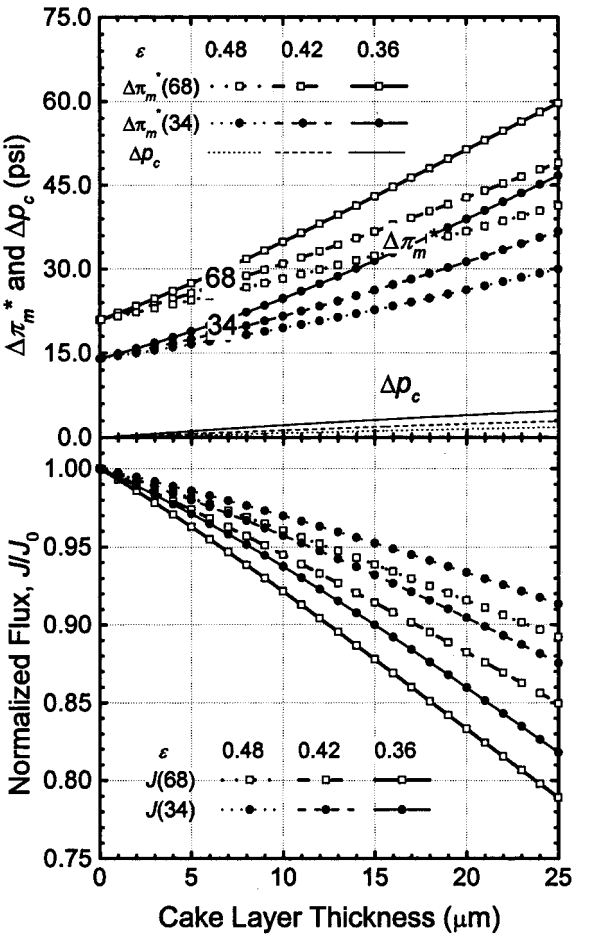

Figure 5. Plot of calculated cake-enhanced osmotic pressure ($\Delta\pi_m$*) and *trans*-cake pressure (Δp_c) as a function of cake layer thickness for several porosities. Mass transfer related effects are simulated using the hydrodynamic conditions described in items (1) and (4) in Table 1. The following parameters used in the calculations: $J_0 = 1.42 \times 10^{-5}$ m/s (30 gfd), $R_m = 10^{-11}$ Pa-s/m; $\Delta P_{34} = 220$ psi and $\Delta P_{68} = 227$ psi; $Q = 0.95$ Lpm; $\gamma_{0,34} = 1336\ s^{-1}$ and $\gamma_{0,68} = 334\ s^{-1}$; $C_b = 0.01$ M NaCl; and $0.97 \geq R_{o,34} \geq 0.96$ and $0.96 \geq R_{o,68} \geq 0.95$.

pressure increases more quickly due to the initial difference in mass transfer. Another factor to consider in actual filtration experiments is that the rate of cake layer growth and the deposit layer porosity may be affected by different tangential shear rates. So, at a given crossflow rate the flux decline in the 68 unit may be even more severe if a thicker or more dense colloid deposit layer is formed.

Relative influence of channel height and shear on colloidal fouling

Preliminary fouling experiments were performed to measure the influence of crossflow membrane filter geometry on colloidal fouling of four commercial RO/NF membranes. Normalized flux decline data (J/J_0) are plotted in Fig. 6 for the hydrodynamic and mass transfer conditions described by items 1 and 4 in Table 1. Open symbols represent data obtained from the 34 unit and closed symbols represent data from the 68 unit. All four membranes were tested at the same physical and chemical operating conditions and feed solution chemistry. These four membranes were chosen to validate the fact that any influence of channel height and shear rate was significant for membranes with different physical and chemical properties. The most important differences in membrane properties were the membrane resistance, which on average was three times greater for the RO membranes, and the salt rejection, which ranged from about 20 to over 95%. At the same feed flow rate, initial osmotic pressure effects in experiments depicted by Fig. 6 were different due to the different channel heights and to the different salt rejections.

The difference in flux decline within the first hour was indistinguishable for all four membranes. After the first hour, flux decline in the 34 unit slowed, and in the 68 unit it continued to decline rapidly for all four membranes. In the 34 unit all four membranes fouled moder-

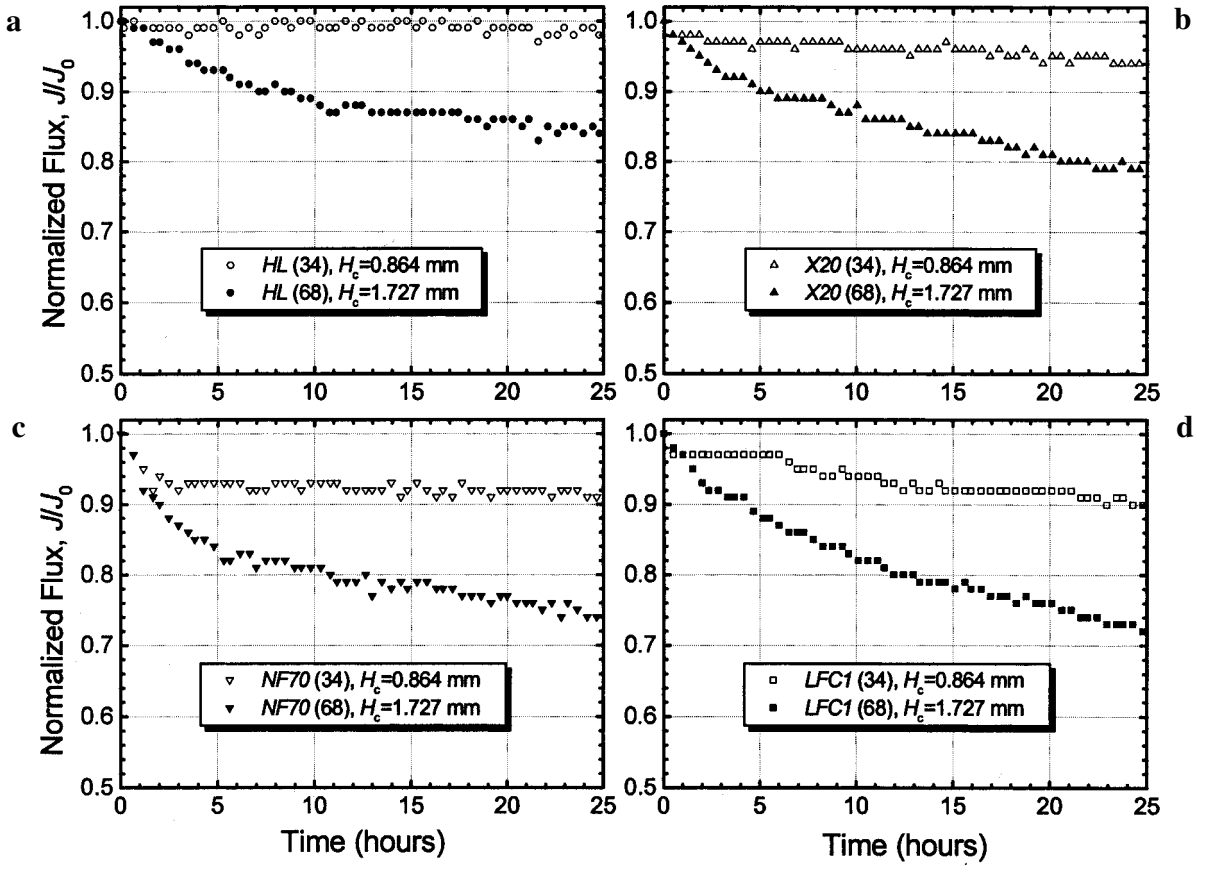

Figure 6. Normalized flux decline data for colloidal fouling experiments conducted with four commercial RO/NF membranes HL (**a**), X20 (**b**), NF70 (**c**), and LFC1 (**d**). All experiments were conducted at constant physico-chemical conditions of 1.4×10^{-5} m/s (30 gfd) initial flux, 0.01 M NaCl, 200 mg/L (0.08% v/v) 100 nm silica colloids, 25°C, and pH 6.8 $\pm$ 0.2. A constant feed flow rate of 0.95 Lpm provided shear rates of 1336 s^{-1} and 334 s^{-1} in the 34 unit (H_c = 0.864 mm) and the 68 unit (H_c = 1.73 mm), respectively.

ately, while in the 68 unit all four membranes fouled severely. Few mechanistic conclusions can be drawn from the limited data presented in Fig. 6, but it is clear that the coupled influence of channel height and shear rate on colloidal fouling was significant, regardless of any differences in membrane properties.

Six additional filtration experiments were conducted in the 34 and 68 units at each of the feed flow rates listed in Table 1. Normalized flux decline data from these experiments are plotted in Fig. 7 (above the break in the *Y*-axis) with corresponding crossflow channel heights and shear rates summarized in the figure key. The reverse osmosis membrane, *LFC1*, was used and all other experimental conditions were the same as in Fig. 6. Open symbols indicate fouling data obtained from the 34 unit and solid symbols indicate data obtained from the 68 unit. The numbers in the figure key correspond to the same item numbers in Table 1.

The flux data from the 34 and 68 units was similar for about 1 h into the experiment, regardless of channel height or shear rate. After this initial period, the flux decline in the 34 unit was distinctly less than that in the 68 unit. Within each filter, the flux at each shear rate was the same for about 8 h. At various times beyond 8 h, measured flux values decrease in order of decreasing shear rate. For example, data from the 68 unit at shear rates of 334 and 1336 s^{-1} resulted in 22 and 28% flux decline, respectively, at 25 h.

Perhaps the most interesting data points in Fig. 7 are those obtained at the same shear rate (1336 s^{-1}) in the 34 and 68 units. The flux decline data are the open triangles and the closed squares, respectively. The dramatic difference in flux decline suggests the possibility that a significantly thicker and/or more compact cake layer formed in the 68 unit. It is also interesting to investigate further the data from the 68 unit at the lowest shear rate (334 s^{-1}) to decipher the sole influence of shear rate on fouling. An iterative solution of Equations (9) and (12) was performed similarly to the calculations described for the theoretical data of Fig. 5. However, in these calculations a porosity of 48% was assumed and cake layer thickness was used to fit the cake layer and cake-enhanced osmotic pressure drops to the measured flux data. All other parameters used in the calculations were identical to those used in determining the theoretical data in Fig. 5.

The resulting cake layer masses (in grams) are plotted below the break on the *Y*-axis of Fig. 7. It is typically assumed that the shear rate limits cake growth in crossflow membrane filtration (Davis, 1992). Indeed, the data of Fig. 7 suggest that more colloids deposited in the 68 unit at the lower shear rate, but only after about 10 h. So, there

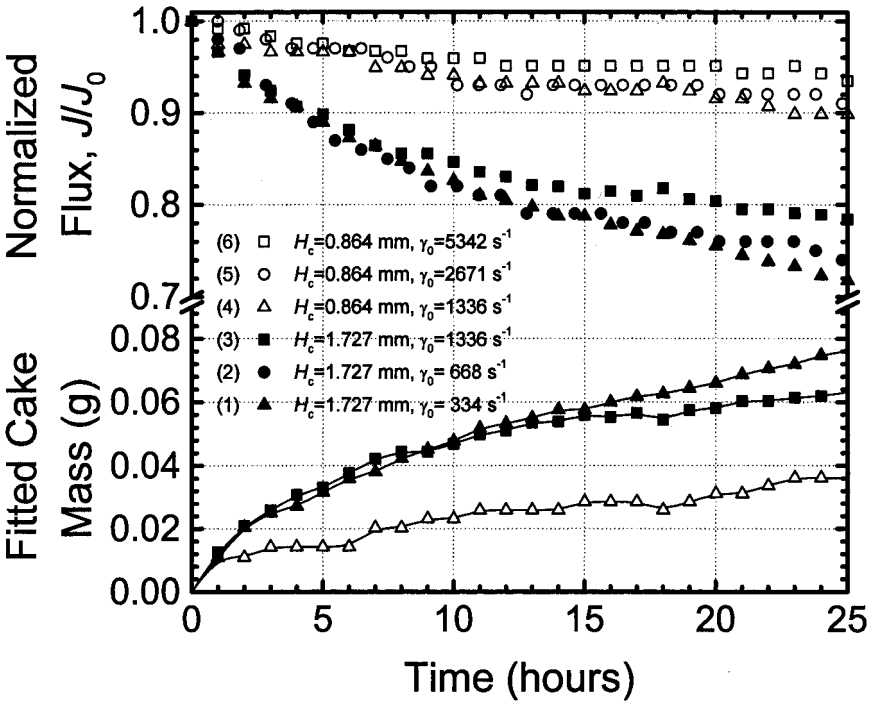

Figure 7. Normalized flux decline and fitted cake mass data for reverse osmosis membrane LFC1 in CMF units with different channel height over a range of feed flow rates, crossflow velocities, and shear rates. All runs in the thin-channeled 34 unit (H_c = 0.864 mm) exhibit less flux decline than those in the 68 unit (H_c = 1.73 mm). Other experimental conditions are as in Fig. 6.

is a period of time for which crossflow did not significantly change the mass of particles deposited. These results were expected and are consistent with previously published experimental colloidal fouling data (Hong *et al.*, 1997). However, fewer colloids deposited in the 34 unit than in the 68 unit at the same shear rate of 1336 s^{-1}, which was not expected and even more interesting. Because porosity and cake mass were both used as fitting parameters, it may be argued that the fitted cake mass values may be arbitrary, hence the need for *in situ* cake mass measurements.

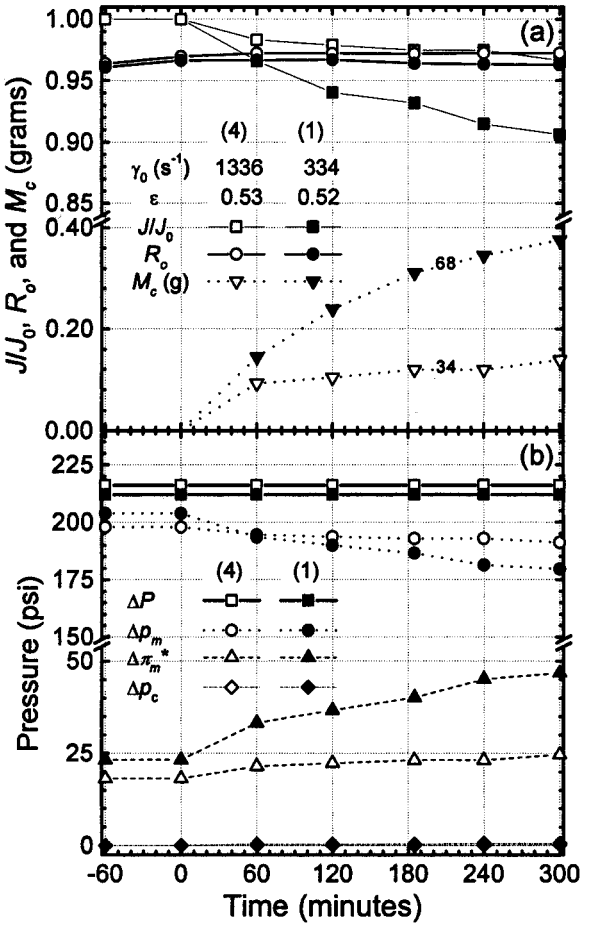

Figure 8. Data for LFC1 from experiments 1 and 4 (Fig. 7) in the 68 and 34 units, respectively, conducted at constant physico-chemical conditions of 1.4×10^{-5} m/s (30 gfd) initial flux, 0.01 M NaCl, 200 mg/L (0.08% v/v) 100 nm silica colloids, 25°C, and pH 6.8 ± 0.2. The feed-flow rate was 0.95 Lpm in both filters resulting in wall shear rates of 334 and 1336 s^{-1} in the 68 and 34 units, respectively. In (**a**) measured values of normalized flux decline (J/J_0), observed salt rejection (R_o), and deposit layer mass (M_c in grams) are plotted against time of filtration. Cake layer mass, M_c, comes from multiplying the deposit layer mass per unit membrane area, M_d, by the membrane area (0.01387 m^2). In (**b**) applied pressure (ΔP), *trans*-membrane pressure (Δp_m), cake-enhanced osmotic pressure ($\Delta \pi_m$*), and *trans*-cake pressure (Δp_c) are plotted against time of filtration.

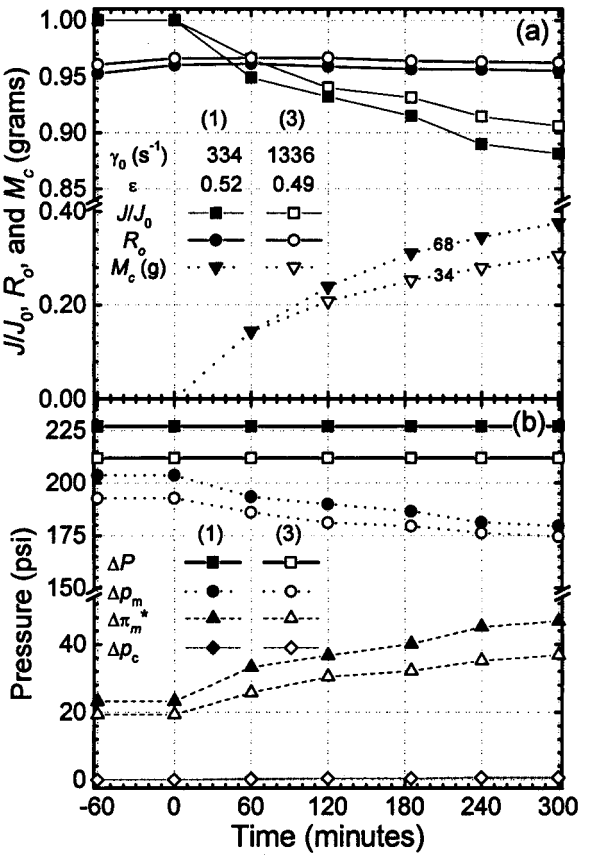

Figure 9. Data for LFC1 from experiments 1 and 3 (Fig. 7) in the 68 unit, conducted at constant physico-chemical conditions of 1.4×10^{-5} m/s (30 gfd) initial flux, 0.01 M NaCl, 200 mg/L (0.08% v/v) 100 nm silica colloids, 25°C, and pH 6.8 ± 0.2. The feed flow rates were 0.95 and 3.8 Lpm resulting in wall shear rates of 334 and 1336 s^{-1}, respectively. In (**a**) measured values of normalized flux decline (J/J_0), observed salt rejection (R_o), and cake layer mass (M_c) are plotted against time of filtration. In (**b**) applied pressure (ΔP), *trans*-membrane pressure (Δp_m), cake-enhanced osmotic pressure ($\Delta \pi_m$*), and *trans*-cake pressure (Δp_c) are plotted against time of filtration.

Verification of the influence of channel geometry and shear rate on colloidal fouling

The three key colloidal fouling experiments from Fig. 7 were repeated, but the particle suspension was fed to only one crossflow membrane filter so that colloid deposit layer mass could be measured as described in the experimental section. These experiments are labeled (1), (3), and (4) in Fig. 7, indicating that the mass transfer properties employed coincide with those labeled by the same item number in Table 1. The results are presented in Figs. 8–10. The starting time in the figures is −60 min,

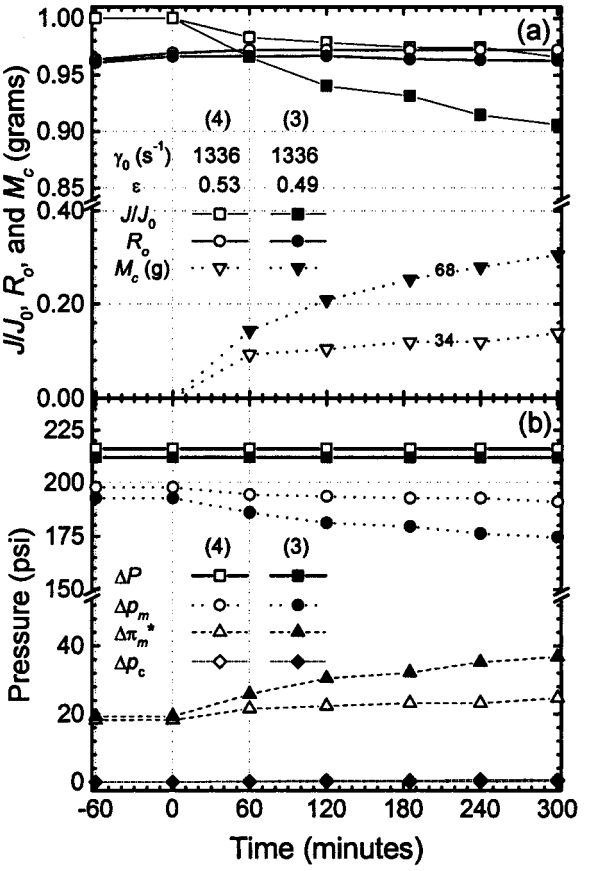

Figure 10. Data for LFC1 from experiments 3 and 4 (Fig. 7) in the 68 and 34 units, respectively, conducted at constant physico-chemical conditions of 1.4×10^{-5} m/s (30 gfd) initial flux, 0.01 M NaCl, 200 mg/L (0.08% v/v) 100 nm silica colloids, 25°C, and pH 6.8 ± 0.2. The feed flow rates were 0.95 and 3.8 Lpm in the 34 and 68 units, respectively, resulting in a fixed shear rate of 1336 s^{-1}. In (**a**) measured values of normalized flux decline (J/J_0), observed salt rejection (R_o), and cake layer mass (M_c) are plotted against time of filtration. In (**b**) applied pressure (ΔP), *trans*-membrane pressure (Δp_m), cake-enhanced osmotic pressure ($\Delta \pi_m^*$), and *trans*-cake pressure (Δp_c) are plotted against time of filtration.

indicating that flux and salt rejection were stable for at least 60 min before addition of silica particles at time equal to zero. The equilibration and mass transfer analyses occurred prior to the 60 min preparticle stabilization period. In part (a) of each figure, the normalized flux, salt rejection, and cake layer mass, M_c (in grams) are plotted against time. Cake layer mass M_c, comes from multiplying the deposit layer mass per unit membrane area, M_d, by the membrane area (0.01387 m^2). In part (b) of the figures, the corresponding pressure drops (applied, membrane, cake, and osmotic) are plotted against the same time scale. The data allows direct comparison of fouling data resulting from different shear rates in different channels (Fig. 8), different shear rates in the same channel (Fig. 9), and the same shear rate in different channels (Fig. 10).

Data from experiments at mass transfer conditions 1 and 4 are plotted in Fig. 8. In these two experiments, channel heights were 0.864 and 1.73 mm, and shear rates were 334 and 1336 s^{-1}, respectively. Cake layer mass was noticeably different 1 h into the experiment, but flux decline was only marginally different. After 5 h, the flux declines to 97 and 90% in the 34 and 68 units, respectively. Flux decline in Fig. 8 is comparable to the corresponding flux decline curves in Fig. 7 (note that data in Fig. 8 are shown for only 5 h). The initial salt rejection is higher in the 34 unit (96.9%) than the 68 unit (95.3%), which was consistent with data observed in previous experiments and assumed in theoretical calculations. Following addition of particles, there was an initial increase in salt rejection, followed by a gradual (slight) decline over the duration of the experiment. The initial increase may be due to disruption of the concentration polarization layer by the first few layers of colloids deposited. After 5 h, the cake layer mass was nearly a factor of four greater in the 68 unit than the 34 unit. The higher shear rate resulting from the lower channel height in the 34 unit appears to limit particle accumulation and cake layer growth.

In Fig. 8(b), the slight difference in applied and *trans*-membrane pressure at the start of the experiment is due to differences in both salt rejection and membrane permeability. The difference in the initial osmotic pressure is assumed due to the different shear rate, which is thought to govern concentration polarization. Cake layers in both filters provide negligible hydraulic pressure drop (Δp_c) regardless of differences in cake layer mass. The substantial difference in cake-enhanced osmotic pressure is primarily due to the greater cake layer mass in the 68 unit, and to a lesser extent the lower mass transfer coefficient. The cake porosity was estimated by minimizing the difference between the osmotic pressures calculated from Equations (9) and (12). The estimated cake layer porosity averaged over 5 h was 53.4 (±2.9) in the 68 unit and 65.9 (±7.9) percent in the 34 unit, which is a significant difference.

In summary, the data of Fig. 8 indicate that the combination of lower channel height and higher shear reduced the initial osmotic pressure and cake layer growth, which led to higher cake porosity, lower cake-enhanced osmotic pressure, higher flux, and higher salt rejection.

Data from experiments at mass transfer conditions 1 and 3 are plotted in Fig. 9. In these two experiments the shear rate was set at 334 s^{-1} (1) and 1336 s^{-1} (3), but the channel height was fixed at 1.73 mm. The flux was

only marginally different after 5 h, declining to 90% and 92% at shear rates of 334 and 1336 s^{-1}, respectively. This is nearly identical to the corresponding data of Fig. 7. The observed salt rejection is slightly higher throughout the entire experiment at the higher shear rate. Again, this may be related as much to variability in membrane properties for different samples of LFC1 as to crossflow hydrodynamics.

Cake layer growth appears unaffected by any difference in shear rate up to about the first hour of particle filtration. This is consistent with the data of Fig. 7, as well as other investigations where the initial stage of colloidal fouling was shown to be independent of crossflow hydrodynamics (Hong *et al.*, 1997). At later times, as expected, slightly less cake mass was deposited at the higher shear rate. The average estimated porosity for these experiments over 5 h were 53.4 ($\pm$2.9) and 50.2 ($\pm$5.4) percent for wall shear rates of 334 and 1336 s^{-1}, respectively, which is not a significant difference.

In Fig. 9(b), the applied pressure is shown to be constant throughout the experiment, and is significantly different due to slight differences in membrane permeability, salt rejection, and crossflow hydrodynamics. The actual *trans*-cake pressure is less than 1 psi after 5 h in either experiment, which is practically negligible. The transient cake-enhanced osmotic pressure drop is lower at the higher flow rate, as predicted by the film-theory (mass transfer was enhanced by the higher shear rate).

In summary, the data of Fig. 9 suggests that increasing shear rate within a given filter reduces the initial osmotic pressure, enhances salt rejection, and marginally reduces cake layer growth, which leads to slightly higher flux.

Data from experiments at mass transfer conditions 3 and 4 are plotted in Fig. 10. In these experiments, the shear rate was fixed at 1336 s^{-1} for channel heights of 0.864 (34 unit) and 1.73 mm (68 unit). At the same shear rate nearly identical initial salt rejection and osmotic pressure resulted. This is consistent with film-theory predictions. However, significantly more cake mass deposited on the membrane in the 68 unit. The average porosity over 5 h was estimated to be 50.2 ($\pm$5.4) and 65.9 ($\pm$7.9) percent in the 68 and 34 units, respectively, which is a significant difference. A more compact cake with nearly double the mass formed in the crossflow membrane filter with greater channel height.

The applied pressures were roughly the same in this case (212 psi in the 68 unit, 216 psi in the 34 unit). The difference was almost entirely due to the pure water permeability of the two membrane coupons. The difference in initial *trans*-membrane osmotic pressure was 1 psi, which is explained by the slight difference (0.2%) in initial salt rejection and the difference in experimental CP modulus previously discussed. The *trans*-cake pressure is below 1 psi in both units, proving to be essentially negligible compared to cake-enhanced osmotic pressure.

In summary, the lower channel height significantly reduced both osmotic pressure effects and cake layer growth, which resulted in higher salt rejection and less flux decline. A potential explanation for these results lies in analysis of the corresponding cake layer thicknesses with respect to the channel heights. The predicted and experimental film layer thickness and cake layer thickness for Experiments 1, 3, and 4 are compared in Table 2. First, film-theory under predicted the concentration polarization layer thickness. Second, the cake thickness is between 8 and 18% of the experimental film layer thickness, which supports the hindered diffusion model assumption of a relatively thin cake layer for the duration of the experiments in this study.

The key information to be derived from the data of Table 2 is the ratio of cake layer thickness to channel height (at 5 h). Cake layer thickness is calculated from $\delta_c = M_d/\rho_c\,(1 - \varepsilon)$ (Faibish *et al.*, 1998). The percent of the channel (height) occupied by the cake layer was the same when the shear rate was the same, even though channel height varied by a factor of 2. The percent of the channel (height) occupied by the cake layer was different when the shear rate was different. The shear-limited cake growth is consistent with past investigations of colloidal fouling in microfiltration (Davis, 1992). The significance is confirmation that the tangential flow field

Table 2. Film layer and colloid cake layer thicknesses for filtration experiments of Figs. 8–10.

Item no.	*CMF unit*	H_c *[μm]*	u *[cm/s]*	γ_0 *[s^{-1}]*	$\delta_{f,th}$[a] *[μm]*	$\delta_{f,ex}$[b] *[μm]*	$\delta_{c,ex}$[c] *[μm]*	ε_c[d] *[%]*	$\delta_{f,th}/H_c$ *[−]*	$\delta_{f,ex}/H_c$ *[−]*	$\delta_{c,ex}/H_c$ *[−]*
1	68	1,727	9.6	334	126	139	25	53	7.3%	8.0%	1.4%
3	68	1,727	38.4	1,336	79.2	117	19	50	4.6%	6.8%	1.1%
4	34	864	19.2	1,336	79.2	109	9.2	66	9.2%	13%	1.1%

[a]Theoretical film layer thickness according to Equation (10); [b]experimental film layer thickness according to Equation (8); [c]experimental cake layer thickness (at 5h) derived from Equations (12) and (15); [d]experimental cake layer porosity (at 5h) derived from Equations (12) and (15).

was sensitive to thin deposit layers (≈1% of channel height).

CONCLUSION

Laboratory-scale crossflow membrane filters with different channel heights were used to test the influence of channel height and shear rate on colloidal fouling of salt rejecting membranes. The cake-enhanced osmotic pressure model was used to predict the effect of colloid deposit layers on both flux decline and salt rejection. When combined with cake layer mass measurements, the model provided a more complete picture of the role of crossflow channel height and shear rate in colloidal fouling.

Within a crossflow membrane filter of fixed channel height, increasing shear rate decreased the initial osmotic pressure drop, colloid deposition, and resultant flux decline, while salt rejection was enhanced. At constant volumetric feed flow rate, higher shear in the filter with reduced channel height dramatically reduced the initial osmotic pressure drop, colloid deposition, and flux decline. At a fixed shear rate, the initial salt rejection and osmotic pressure drops were nearly identical in filters with different channel heights. However, the primary mechanism of flux decline, cake-enhanced osmotic pressure, was substantially higher in the filter with greater channel height. Even though the same shear rate was applied, the deposit layer growth and extent of fouling was limited by the channel height. Finally, by reducing channel height all mechanisms of flux decline were reduced—initial osmotic pressure, *trans*-cake hydraulic pressure, and cake-enhanced osmotic pressure, while salt rejection was enhanced.

ACKNOWLEDGMENTS

The authors would like to acknowledge the financial support of the American Water Works Association Research Foundation, the National Science Foundation (Grant BES-0114527), and the Yale Institute of Biospheric Studies. The authors would also like to thank Hydranautics, Dow-FilmTec, Trisep, and Osmonics for supplying membranes and Nissan Chemical America Corp. for providing the colloidal silica particles.

REFERENCES

BHATTACHARJEE, S., CHEN, J.C., and ELIMELECH, M. (2001). Coupled model of concentration polarization and pore transport in crossflow nanofiltration. *AIChE J.* **47,** 2733.

BHATTACHARJEE, S., KIM, A.S., and ELIMELECH, M. (1999). Concentration polarization of interacting solute particles in cross-flow membrane filtration. *J. Colloid Interface Sci.* **212,** 81.

BLATT, W.F., DRAVID, A., MICHAELS, A.S., and NELSON, L. (1970). In: J.E. Flinn, Ed., *Membrane Science and Technology: Industrial, Biological, and Waste Treatment Processes.* Columbus, OH: Plenum Press, p. 47.

BOUDREAU, B.P. (1996). The diffusive tortuosity of fine-grained ulithified sediments. *Geochim. Cosmochim. Acc.* **60,** 3139.

BRAGHETTA, A., DIGIANO, F.A., and BALL, W.P. (1998). Nom accumulation at nf membrane surface: Impact of chemistry and shear. *J. Environ. Eng.-ASCE* **124**, 1087.

CHELLAM, S., and TAYLOR, J.S. (2001). Simplified analysis of contaminant rejection during ground- and surface water nanofiltration under the information collection rule. *Water Res.* **35,** 2460.

DAVIS, R.H. (1992). Modeling of fouling of crossflow microfiltration membranes. *Sep. Purif. Method* **21,** 75.

ELIMELECH, M., and BHATTACHARJEE, S. (1998). A novel approach for modeling concentration polarization in crossflow membrane filtration based on the equivalence of osmotic pressure model and filtration theory. *J. Membr. Sci.* **145,** 223.

ENDO, Y., and ALONSO, M. (2001). Physical meaning of specific cake resistance and effects of cake properties in compressible cake filtration. *Filtr. Sep.* **38,** 43.

EVANGELISTA, F. (1985). A short cut method for the design of reverse-osmosis desalination plants. *Ind. Eng. Chem. Proc. D. D.* **24,** 211.

FAIBISH, R.S., ELIMELECH, M., and COHEN, Y. (1998). Effect of interparticle electrostatic double layer interactions on permeate flux decline in crossflow membrane filtration of colloidal suspensions: An experimental investigation. *J. Colloid Interface Sci.* **204,** 77.

HOEK, E.M.V. (2002). Ph.D. Thesis, Department of Chem. Eng., Yale University, New Haven, CT.

HONG, S., FAIBISH, R.S., and ELIMELECH, M. (1997). Kinetics of permeate flux decline in crossflow membrane filtration of colloidal suspensions. *J. Colloid Interface Sci.* **196,** 267.

HONG, S.K., and ELIMELECH, M. (1997). Chemical and physical aspects of natural organic matter (nom) fouling of nanofiltration membranes. *J. Membr. Sci.* **132,** 159.

KATAOKA, T., TSURU, T., NAKAO, S., and KIMURA, S. (1991). Permeation equations developed for prediction of membrane performance in pervaporation, vapor permeation and reverse-osmosis based on the solution-diffusion model. *J. Chem. Eng. Jpn.* **24,** 326.

MALLEVIALLE, J., ODENDAAL, P.E., and WIESNER, M.R.

(1996). Water treatment membrane processes. In *American Water Works Association Research Foundation, L.D.E., and Water Research Commission of South Africa*. New York: McGraw-Hill.

MASKAN, F., WILEY, D.E., JOHNSTON, L.P., and CLEMENTS, D.J. (2000). Optimal design of reverse osmosis module networks. *AIChE J.* **46,** 946.

MURTHY, Z.V.P., and GUPTA, S.K. (1997). Estimation of mass transfer coefficient using a combined nonlinear membrane transport and film theory model. *Desalination* **109,** 39.

PORTER, M.C. (1972). Concentration polarization with membrane ultrafiltration. *Ind. Eng. Chem. Prod. Res. Dev.* **11,** 234.

SIRKAR, K.K., DANG, P.T., and RAO, G.H. (1982). Approximate design equations for reverse-osmosis desalination by spiral-wound modules. *Ind. Eng. Chem. Prod. Res. Dev.* **21,** 517.

SIRKAR, K.K., and RAO, G.H. (1981). Approximate design equations and alternate design methodologies for tubular reverse-osmosis desalination. *Ind. Eng. Chem. Prod. Res. Dev.* **20,** 116.

SONG, L., and ELIMELECH, M. (1995). Theory of concentration polarization in crossflow filtration. *J. Chem. Soc. Faraday Trans.* **91,** 3389.

VAN DER MEER, W.G.J., and VAN DIJK, J.C. (1997). Theoretical optimization of spiral-wound and capillary nanofiltration modules. *Desalination* **113,** 129.

VOROS, N.G., MAROULIS, Z.B., and MARINOSKOURIS, D. (1997). Short-cut structural design of reverse osmosis desalination plants. *J. Membr. Sci.* **127,** 47.

VRIJENHOEK, E.M., ELIMELECH, M. and HONG, S. (2001). Influence of membrane surface properties on initial rate of colloidal fouling of reverse osmosis and nanofiltration membranes. *J. Membr. Sci.* **188,** 115.

WIJMANS, J.G. and BAKER, R.W. (1995). The solution-diffusion model—A review. *J. Membr. Sci.* **107,** 1.

WILEY, D.E., FELL, C.J.D., and FANE, A.G. (1985). Optimization of membrane module design for brackish water desalination. *Desalination* **52,**YIANTSIOS, S.G., and KARABELAS, A.J. (1998). The effect of colloid stability on membrane fouling. *Desalination* **118,** 143.

ZHU, X., and ELIMELECH, M. (1997). Colloidal fouling of reverse osmosis membranes: Measurements and fouling mechanisms. *Environ. Sci. Technol.* **31,** 3654.

ZHU, M.J., ELHALWAGI, M.M., and ALAHMAD, M. (1997). Optimal design and scheduling of flexible reverse osmosis networks. *J. Membr. Sci.* **129,** 161.

ZYDNEY, A.L. (1997). Stagnant film model for concentration polarization in membrane systems. *J. Membr. Sci.* **130,** 275.